Ice Concentration Scaling Laws for Freshwater Lakes in Numerical Weather and Climate Prediction

Murray Mackay[1]

[1]Environment and Climate Change Canada

March 26, 2023

Abstract

If lake ice is assumed to deform and fail as a linear viscoelastic material under the action of wind stress, then a simple ice concentration scaling law can be constructed suitable for one-dimensional lake models embedded within environmental prediction systems. Most 1-D lake models assume no ice mechanics at all, while others adapt the viscous-plastic rheology common in ice-ocean models for the purpose of estimating ice fraction. Elastic buckling is generally disregarded as a significant failure mechanism in ice under low stress conditions at geophysical scales. However, by adding viscosity to the constitutive equation, the conditions for viscoelastic buckling seem quite plausible over a wide range of lake size and ice thickness. An ice concentration scaling law based on this process is evaluated here in multiannual simulations over North America and found to produce superior ice phenology statistics compared with simulations based on plastic failure or no ice mechanics.

Ice Concentration Scaling Laws for Freshwater Lakes in Numerical Weather and Climate Prediction

Murray D. MacKay[1]

[1]Meteorological Research Division, Environment and Climate Change Canada, Toronto, Canada

Corresponding author: Murray MacKay (murray.mackay@ec.gc.ca)

Key Points:

- Most one-dimensional lake models neglect ice mechanics or assume plastic failure, and frequently perform poorly regarding ice phenology.
- Assuming lake ice fails as a linear viscoelastic material at geophysical scales leads to a simple parameterization of ice concentration.
- The new scheme outperforms plastic failure or the absence of mechanics with respect to ice – on and ice duration.

Abstract

If lake ice is assumed to deform and fail as a linear viscoelastic material under the action of wind stress, then a simple ice concentration scaling law can be constructed suitable for one-dimensional lake models embedded within environmental prediction systems. Most 1-D lake models assume no ice mechanics at all, while others adapt the viscous-plastic rheology common in ice-ocean models for the purpose of estimating ice fraction. Elastic buckling is generally disregarded as a significant failure mechanism in ice under low stress conditions at geophysical scales. However, by adding viscosity to the constitutive equation, the conditions for viscoelastic buckling seem quite plausible over a wide range of lake size and ice thickness. An ice concentration scaling law based on this process is evaluated here in multiannual simulations over North America and found to produce superior ice phenology statistics compared with simulations based on plastic failure or no ice mechanics.

Plain Language Summary

Most mid- and high- latitude lakes experience periods of partial ice cover (*i.e.* ice concentration < 100%) during early winter. While very small lakes might freeze solid in a single night under calm conditions, larger lakes may take days or weeks to completely freeze because wind stress continually breaks the ice cover resulting in patches of open water. The extent of wintertime open water is very important for both lake ecology and for regional weather conditions (*e.g.* lake-effect snowstorms). Many weather and climate models employ one-dimensional lake models that do not represent fractional ice cover at all, or parameterize it based on mechanical ideas from sea ice models, resulting in poor timing and duration of simulated ice cover. Here we propose a new scheme based on different mechanics that improves these simulated features.

1 Introduction

The interface between a lake and the overlying atmosphere regulates flux exchange between the two, and the state of ice at the lake surface – both in terms of thickness and concentration (*i.e.* fractional cover) – is the predominant governing factor for much of the year in high- and mid-latitude regions. Areas of thick ice, especially if snow covered, severely restrict the transmission of shortwave radiation and gas exchange with obvious impacts on lake ecology.

On the other hand many lakes experience only partial ice cover for much (if not all) of the winter, and patches of open water can lead to for example surface oxygen renewal and nutrient redistribution (through circulation) and increased primary production (through increased light penetration), not to mention major fluxes of heat and moisture into the generally cold, dry air above. It is clear that climate and numerical weather prediction modelling systems that incorporate some representation of lakes need to consider the nature of lake ice carefully, especially under conditions of fractional cover. For modelling systems that employ 3-dimensional lake models with fully dynamic ice schemes (*e.g.* Durnford et al., 2018) this is generally not a problem. However, many forecasting systems represent lakes with simple one-dimensional thermodynamic models, for which ice mechanics must be parameterized in order to simulate the correct balance of ice cover and open water.

One – dimensional lake schemes have been used in a number of short-range forecasting studies that examined ice conditions (*eg.* Rontu et al., 2019; Eerola et al., 2014; Balsamo et al., 2012). In all of these studies ice-on tended to occur too early, at least partially due to the fact that the lake scheme employed (FLake – Mironov et al., 2010) did not represent fractional ice cover. In this scheme, once ice grows to a thickness of 1 mm it is assumed to cover the entire lake (or gridcell for large lakes). In reality such ice is easily broken by wind or waves and rafted, resulting in both open water and ice-covered areas. However, the period of partial ice cover may be short lived for small lakes and larger lakes could benefit from data assimilation – at least for short range forecasts.

The situation is more problematic for long range forecasts and climate simulations. In a climate modelling study over Northern Europe based on the Max Plank Institute's REMO coupled with FLake, Pietikäinen et al. (2018) found ice-on dates were again too early: 2-3 weeks for moderately sized (100 – 1000 km^2) Finnish lakes, but more than 1 month early for Lakes Vättern (1912 km^2) and Onega (9700 km^2) and more than 2 months early for Lake Ladoga (17,700 km^2). In Le Moigne et al. (2016), ice-on is not evaluated *per se* though the authors discuss the necessity of setting ice and snow albedos arbitrarily low in FLake in order to account for radiative impacts of fractional ice cover. This issue was also noted by Subin et al. (2012) for the Lake, Ice, Snow, and Sediment Simulator (LISSS), a one – dimensional lake model that also neglects fractional ice cover. In addition, while ice-on dates were not evaluated extensively, this study did note that ice-on occurred several weeks too early for their simulation of Great Slave Lake.

Below we propose a simple approach to represent ice concentration in any 1-dimensional lake model. The key ingredient is the determination of a critical ice thickness above which ice concentration tends to remain stable at 100%. Below this thickness ice is assumed to break and ridge or raft, resulting in the presence of some open water.

2 A Universal Scaling Law for Critical Lake Ice Thickness?

Open water leads in ice cover (for both lakes and oceans) are frequently generated under the action of wind stress that mechanically breaks sufficiently thin ice and forces the rubble into ridges (*e.g.* Hopkins, 1998) a process that has been successfully represented in a modelling study of Lake Peipsi by Leppäranta and Wang (2008). Following Hibler (1979), Leppäranta and Wang view ice as a viscous-plastic medium with a yield strength given by

$$P = P^{*} h\, exp\{-C(1-A)\} \qquad (1),$$

where h is the mean ice thickness, A is the ice compactness, C is a strength reduction factor, and P^* is the compressive strength of compact ice (per unit thickness). Leppäranta and Wang (2008) suggest these last two parameters be >>1 and 10-100 kPa respectively. When fully compact (*i.e.* A=1) the ice will break due to wind stress τ_a when

$$h < H = \left(\frac{\tau_a}{P^*}\right) L \qquad (2),$$

where L is taken as the fetch over the lake. When ice thickness is greater than this critical threshold it is considered stable; when it is thinner it breaks and forms pressure ridges and open water leads. An order of magnitude argument suggests that for wind stress ~ 0.15 Pa and P^* = 27.5 kPa (*e.g.* Hibler & Walsh, 1982) we get $H \approx 5.4\, x 10^{-6} L$. Thus for Lake Peipsi with a mean fetch of about 50 km, Leppäranta and Wang (2008) find that ice is “movable” (*i.e.* subject to mechanical breakup and ridging) when it is thinner than about 27 cm, and stable when it is thicker, in agreement with observations.

At first glance this relationship between critical ice thickness H and fetch L may seem reasonable as larger ice fields would sustain more wind stress and thus require greater thickness to be mechanically stable. However (2) clearly fails for very large lakes. Great Bear and Great Slave lakes in northern Canada have mean fetch on the order of 170 km, yet both lakes routinely freeze solid with ice thicknesses of only 55 – 65 cm, whereas (2) implies 93 cm. Leppäranta and Wang (2008) (see also Kirillin et al., 2012) emphasized that P^* could be tuned based on data. However, tuning (2) for Great Bear and Great Slave lakes degrades results for Lake Peipsi (see below).

A scaling law based on (2), however, is not the only choice. For example, if elastic buckling was deemed important prior to ridging then the strength of ice (e.g. Parmerter, 1974) is given by

$$P = \left(\frac{E\rho_w g H^3}{12(1-\upsilon^2)}\right)^{1/2} \qquad (3),$$

where E and ν are the Young's modulus and Poisson's ratio for ice, ρ_w is the density of water, and g is the acceleration due to gravity. This follows from treating the ice cover as a thin plate floating on an elastic (*i.e.* Winkler) foundation (Hetenyi, 1946). Because this would lead to ice much stronger than (2), Rothrock (1975) appears to rule out elastic buckling as an important mechanism in ridging, a sentiment echoed in Schulson (2004).

Other studies have retained the buckling process, though there has been considerable latitude with respect to the value of the Young's modulus selected. Parmerter (1974, 1975) found that 0.3 GPa gave good results in a study of sea ice rafting. Hopkins (1998) chose E = 0.1 GPa in order to achieve reasonable results in an ice ridging model. On the other hand Parmerter and Coon (1972) found that E = 1 GPa worked well for their ridging model.

Now from (3) we find that

$$L\tau_a = \left(\frac{E\rho_w g H^3}{12(1-\upsilon^2)}\right)^{\frac{1}{2}} \qquad (4)$$

becomes

$$H = \left[\frac{\tau_a}{\alpha E^{1/2}}\right]^{2/3} L^{2/3} \qquad (5)$$

where

$$\alpha = \left[\frac{\rho_w g}{12(1-\nu^2)}\right]^{1/2} = 29.96\ [\mathrm{Pa}^{1/2} m^{-1/2}]$$

assuming ν = 0.3 (Gammon et al., 1983).

There are scant relevant observed data to verify these scaling laws for a critical ice thickness over lakes, primarily because of the difficulty in safely measuring ice thickness under conditions of incomplete or marginally complete ice cover. Somewhat fortuitously, the Canadian Ice Service (CIS), has observed weekly ice concentration data from over 100 North American lakes since about 1995, and weekly ice thickness data from two measurement programs (1947-2002; 2002-2020) over a few lake and ocean locations. All three programs are independent and served different objectives, though there is some overlap for three important lakes – Great Bear Lake (31,153 km^2), Great Slave Lake (27,200 km^2) and Baker Lake (1887 km^2), which we have plotted in Fig. 1.

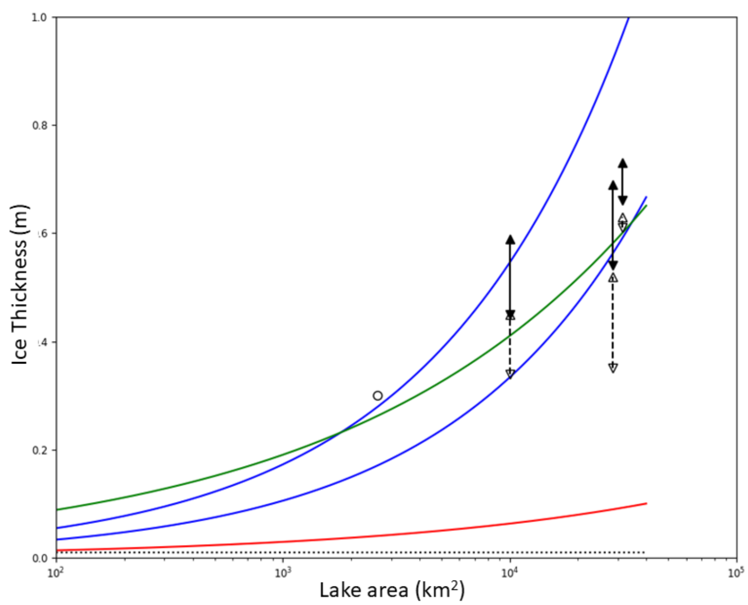

Fig. 1 Critical ice thickness as a function of lake area. Black vertical lines and symbols represent observed estimates. Blue curves represent plastic failure (2) with P^* = 27.5 kPa (upper curve) and P^* = 45 kPa (lower curve). Red curve represents elastic buckling failure (5) with E = 1 GPa. Green curve represents viscoelastic buckling failure (11) with E = 9.0 GPa, $\eta = 10^{11}$ $kg\ m^{-1} s^{-1}$, and assuming steady wind forcing for 6 hours. All solid curves assume wind stress ~ 0.15 Pa. Fetch is estimated as the square root of lake area. The dotted horizontal black line represents a threshold of 1.0 cm for complete ice cover (*i.e.* no ice mechanics). See text for details.

In this figure, solid vertical black lines ending with filled triangles represent the interquartile range of ice thickness when ice concentration was first recorded as 100% (Great Bear Lake: n=4; Great Slave Lake: n=14; Baker Lake: n=16). The vertical black dashed lines ending with unfilled triangles represent the interquartile range of ice thickness when ice concentration was last recorded as 90% (Great Bear Lake: n=4; Great Slave Lake: n=12; Baker Lake: n=15). Thus we estimate that the average critical ice thickness when these lakes first reached 100% ice cover is approximately midway between these solid and dashed segments. Lake Peipsi (2611 km^2) is also indicated in Fig. 1 (open circle) near the point of marginally complete ice cover. Note that in this figure mean lake fetch L is estimated as the square root of lake area, with the exception of Baker lake which is highly elongated in the east-west direction, roughly 100 km in extent.

Fig. 1 also shows the scaling models described above. The blue curves show (2) with: P^* = 27.5 kPa (upper curve), and P^* = 45 kPa (lower curve). Neither curve is consistent with all of the observed data presented. Elastic buckling failure (5) is represented by the red curve. Even assuming the Young's modulus as low as E = 1 GPa, the ice is still much stronger than the observed data suggest.

2.1 The Viscoelastic Buckling of Lake Ice

The condition for classical elastic buckling of a floating thin plate (3) due to some axial force F can be written

$$\left(\frac{\rho_w g H^3}{12(1-\upsilon^2)}\right)^{1/2} E^{1/2} = F. \qquad \textbf{(6)}$$

Classical buckling is generally understood as a bifurcation in the equilibrium condition of the structure in question, where the buckled solution is infinitesimally close to the unbuckled solution (*e.g.* Flügge, 1962, ch. 44). Buckling in and of itself does not necessarily imply *failure* – in our context the actual breakage and ridging or rafting of ice – though this is generally tacitly assumed for thin sheets of ice. A rigorous post-bucking analysis would require a nonlinear finite amplitude theory (*e.g.* Biot, 1965), beyond the scope of this study. As a first step here we extend the linearized, small amplitude stability analysis of thin elastic (floating) sheets of ice into the viscoelastic realm and assume failure to occur shortly after the conditions for buckling are met.

The generalization of elasticity theory to viscoelastic materials can be achieved for a large class of problems by way of a *correspondence principle*, first elucidated by Alfrey (1944), Biot (1954), and Lee (1955). In viscoelasticity, the constitutive equations are generalized based on linear differential operators (P(t), Q(t)) of the rheological model selected, introducing a time dependence to the governing equations. It has long been recognized that taking the Laplace transform of the viscoelastic equations renders a set of equations in transform space formally identical to a corresponding elastic problem if E in the elastic system is replaced by $\hat{Q}(s)/\hat{P}(s)$ in the transformed problem where $\hat{Q}, \hat{P}$ are the Laplace transforms of Q, P respectively. To solve the viscoelastic problem one simply needs to compute the inverse Laplace transform once this substitution is made.

Thus in Laplace transform space, the condition for viscoelastic instability corresponding to (6) becomes

$$\left(\frac{\rho_w g H^3}{12(1-\upsilon^2)}\right)^{1/2}\left(\frac{\hat{Q}(s)}{\hat{P}(s)}\right)^{1/2} = \hat{F}(s) \qquad \textbf{(7)}$$

where $\hat{F}(s)$ is the Laplace transform of the wind forcing F(t), now in general a function of time. This can be solved by inverse Laplace transform once a suitable rheological model is selected. A simple choice that includes both elastic and creep deformation is the Maxwell fluid, represented by

$$\hat{P}(s) = 1 + \frac{\eta}{E}s; \qquad \hat{Q}(s) = \eta s,$$

where η is a viscosity. Now (**7**) becomes

$$\left(\frac{\rho_w g H^3}{12(1-\upsilon^2)}\right)^{1/2} = \frac{1}{\sqrt{\eta}}\hat{F}(s)\hat{G}(s)\ , \qquad \textbf{(8)}$$

where

$$\hat{G}(s) = \left(\frac{1+\frac{\eta}{E}s}{s}\right)^{1/2}$$

has the inverse Laplace transform

$$G(t) = \frac{1}{2}\left(\frac{E}{\eta}\right)^{1/2} \exp\left(-\frac{1}{2}\frac{E}{\eta}t\right)\left[I_0\left(\frac{1}{2}\frac{E}{\eta}t\right) + I_1\left(\frac{1}{2}\frac{E}{\eta}t\right)\right] \qquad ;\ t>0. \quad \textbf{(9)}$$

where I_0 and I_1 are modified Bessel functions of the first kind. It is important to notice that (9) is valid only for t>0; the case for t=0 must be handled separately and added. It is clear on physical grounds that for t=0 we expect to recover the purely elastic case. For now we must add an unknown function G_0 to the RHS of (9), evaluated below, to solve over the full time domain.

By the convolution theorem of Laplace transforms, (8) with (9) becomes after inversion

$$\left(\frac{\rho_w g H^3}{12(1-\upsilon^2)}\right)^{1/2} = \frac{1}{\sqrt{\eta}}\left\{\int_{0^+}^{t} F(t-\tau)G(\tau)\,d\tau + G_0\right\}$$

$$= \frac{\sqrt{E}}{2\eta}\int_{0^+}^{t} F(t-\tau)\exp\left(-\frac{1}{2}\frac{E}{\eta}\tau\right)\left[I_0\left(\frac{1}{2}\frac{E}{\eta}\tau\right) + I_1\left(\frac{1}{2}\frac{E}{\eta}\tau\right)\right]d\tau + \frac{G_0}{\sqrt{\eta}}\ . \qquad \textbf{(10)}$$

This represents the general condition for linear viscoelastic buckling of a Maxwell material under some time dependent wind forcing F(t). Notice that both the material constants E, η, as well as the time history of the forcing are relevant to the buckling criterion. This distinguishes it from the purely elastic case which is instantaneous - it either buckles or it doesn't – depending on E, and the instantaneous magnitude (not the time history) of the applied force.

Consider now the case of a steady wind stress applied at t=0, so that

$$F(t) = L\tau_a \mathcal{H}(t)$$

where $\mathcal{H}(t)$ is the unit Heaviside function. For this case (10) becomes

$$\left(\frac{\rho_w g H^3}{12(1-\upsilon^2)}\right)^{\frac{1}{2}} = L\tau_a \frac{\sqrt{E}}{2\eta}\int_0^t \exp\left(-\frac{1}{2}\frac{E}{\eta}\tau\right)\left[I_0\left(\frac{1}{2}\frac{E}{\eta}\tau\right) + I_1\left(\frac{1}{2}\frac{E}{\eta}\tau\right)\right]d\tau + \frac{G_0}{\sqrt{\eta}}$$

$$= \frac{L\tau_a}{\sqrt{E}}\left\{-1 + \exp\left(-\frac{1}{2}\frac{E}{\eta}t\right)\left[\left(\frac{E}{\eta}t + 1\right) I_0\left(\frac{1}{2}\frac{E}{\eta}t\right) + \left(\frac{E}{\eta}t\right) I_1\left(\frac{1}{2}\frac{E}{\eta}t\right)\right]\right\} + \frac{G_0}{\sqrt{\eta}}$$

It is clear that if we select $G_0 = L\tau_a\sqrt{\frac{\eta}{E}}$ then this becomes

$$\left(\frac{E\rho_w g H^3}{12(1-\upsilon^2)}\right)^{\frac{1}{2}} = L\tau_a\left\{\exp\left(-\frac{1}{2}\frac{E}{\eta}t\right)\left[\left(\frac{E}{\eta}t + 1\right) I_0\left(\frac{1}{2}\frac{E}{\eta}t\right) + \left(\frac{E}{\eta}t\right) I_1\left(\frac{1}{2}\frac{E}{\eta}t\right)\right]\right\} \quad \textbf{(11)}$$

which reduces to the elastic buckling condition (6) for t=0 as required. Note that for the Maxwell model the elastic limit is also recovered for $\eta \to \infty$, so we consider (11) the viscoelastic generalization of (6) for the Maxwell model under steady wind forcing. For finite values of η but on short timescales, series expansions of the exponential and modified Bessel functions suggest

$$\left(\frac{E\rho_w g H^3}{12(1-\upsilon^2)}\right)^{\frac{1}{2}} \approx L\tau_a\left\{1 + \frac{1}{2}\frac{E}{\eta}t\right\}; \quad \frac{E}{\eta}t \ll 1$$

Taking E = 9.0 GPa and η = 10^{11} $kg\ m^{-1}s^{-1}$ (*e.g.* Staroszczyk & Hedzielski, 2004) this approximation requires t << 22 s. Thus for wind forcing on synoptic timescales this condition, which could be called *nearly elastic* bucking, does not seem relevant, though it may be appropriate for other types of linear viscoelastic problems (*e.g.* slowly colliding ice plates). If we consider a steady wind stress (0.15 Pa) acting on the ice field for 6 hours, then the term in the curly brackets in (11) evaluates to 49.75. This is represented by the green curve in Fig. 1 which fits the data much better than the other models. Note we do not require a full 6 hours of steady wind to achieve buckling here. The linear form of (10) indicates that a series of shorter but stronger wind gusts would achieve the same thing. This is clear if F in (10) is replaced with a series of pulses represented by positive and negative Heaviside step functions, perhaps of different amplitudes.

Ice thickness data near the time of freeze-up are difficult to come by. On the other hand, ice concentration data are much more readily available, which we can relate to ice failure through numerical simulation. In the following section we discuss a series of simulations that parameterize ice mechanics based on (2) or (11) described above, as well as the absence of mechanics. As will become clear, the impact of these schemes on fractional ice cover is dramatic. We evaluate these simulations based on Canadian Ice Service observed ice concentration data from 115 lakes over North America in order to help select the optimal approach.

3 Simulations

Recently Garnaud et al. (2022) described simulations of Environment and Climate Change Canada's Surface Prediction System (SPS), which had incorporated a one – dimensional thermodynamic lake scheme. Ice mechanics was parameterized following (2) above, *i.e.* when $\boldsymbol{h} \geq \boldsymbol{H}$ the ice cover was considered complete (fractional ice cover F_{ice} = 1.0), and when $\boldsymbol{h} < \boldsymbol{H}$ the fractional ice cover was computed as $F_{ice} = h/H$. This simple linear approach has been used to parameterize, for example, fractional snow cover in the Canadian Land Surface Scheme (CLASS) for many years (*e.g.* Verseghy, 2017). The compressive strength of ice P^* was set to 27.5 kPa, as in Leppäranta and Wang (2008). Simulations ran on a 2.5 km horizontal resolution grid covering most of Canada and the northern U.S.A. from 1 September 2015 – 31 December 2018. It was found that the new lake scheme improved ice phenology for the smallest lakes, compared with the existing approach (which was largely based on data assimilation), but that this improvement degraded as lake surface area increased. In terms of ice mechanics this behavior could be anticipated from our Fig. 1 (upper blue curve) where it is clear that (2) will produce fractional ice cover for the largest lakes when observations suggest that ice cover is complete (see also below).

Here we perform an identical simulation to that of Garnaud et al. (2022), except we drive SPS with a slightly improved atmospheric and precipitation forcing data set (Gasset et al., 2021).

In addition to parameterizing ice mechanics based on plastic failure (2), we also include simulations based on viscoelastic buckling failure (11), and by assuming no mechanics at all. This last criterion is achieved by setting ice concentration to 100% when ice thickness reaches 1.0 cm (Fig. 1 black dotted curve), similar to the approach used in FLake as noted above.

Ice concentration from all 3 simulations is evaluated against observations from the CIS, examples of which are illustrated in Fig. 2. Fig. 2a shows weekly results for Great Bear Lake, the largest lake in the data set at 31,153 km^2. For each of the 3 winter periods examined, ice-on is clearly too early in the simulation without mechanics (magenta crosses), and too late (or absent) in the simulation assuming plastic failure (blue circles), while the simulation assuming viscoelastic mechanics is better in this respect (green diamonds). For La Grande Reservoir (Fig. 2b – 2835 km^2) ice – on is again several weeks too early in the simulation without mechanics, while the other simulations show nearly identical (and much better) results. Finally, Fig. 2c shows results for a smaller lake – Leech Lake (417 km^2). Ice – on in the simulation without mechanics is still too early. The other simulations are again similar, but examination of especially the 2017/18 winter reveals that ice – on is also too early in the simulation assuming plastic failure while it is better in the viscoelastic simulation. All of these results could have been anticipated from Fig. 1: the viscoelastic ice is harder than the plastic ice for lakes larger than about 2000 km^2 (green curve lies below the upper blue curve), and softer for lakes smaller

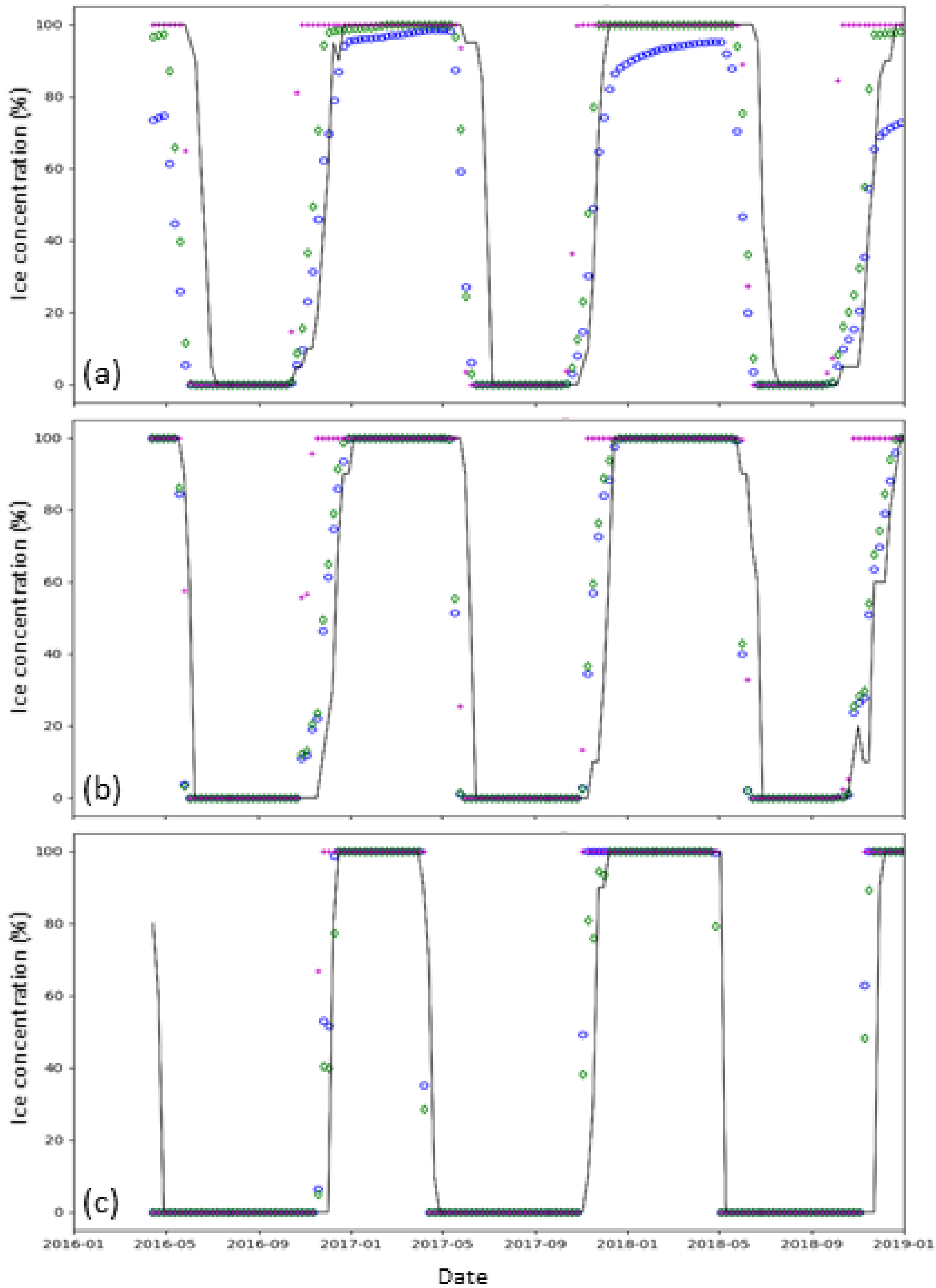

Fig. 2 Observed (thin black curves) and simulated ice concentration (January 2016 – January (2019) for: (a) - Great Bear Lake (31153 km^2); (b) - La Grande Reservoir (2835 km^2); and (c) – Leech Lake (417 km^2). Simulated values assume plastic failure with P^* = 27.5 kPa (blue circles); Viscoelastic buckling failure (green diamonds); and no mechanics (magenta crosses).

than 2000 km^2 (green curve lies above the upper blue curve). For lakes around 2000 km^2 in area both mechanical models produce similar results.

Fig. 3 summarizes ice phenology biases for all 115 lakes for which we have CIS data during this period. Results are separated based on lake size, as suggested above, where “small” refers to areas less than 2000 km^2 and “large” refers to lakes larger than this threshold. Based on this partition, the CIS data set contains 96 small and 19 large lakes. Because the CIS ice concentration observations are weekly and in units of tenths, ice – on (Fig. 3a) is defined as the first week of 90% ice cover, and ice cover duration (Fig. 3b) is defined as the number of weeks of $\geq$ 90% ice cover. On average the viscoelastic model outperforms the other simulations in both metrics for both small and large lakes: ice-on bias is only -8 days (small) and 1 day (large), compared with -12 days, 14 days (plastic), and -21 days, -32 days (no mechanics). Likewise, viscoelastic ice cover duration bias is only 3 days, -18 days (small, large) compared with 7 days, -34 days (plastic), and 22 days, 24 days (no mechanics). Note that none of the models handles the ice – off process particularly well (not shown). Differences due to the mechanics of melting, rotten, isothermal ice have not been considered here.

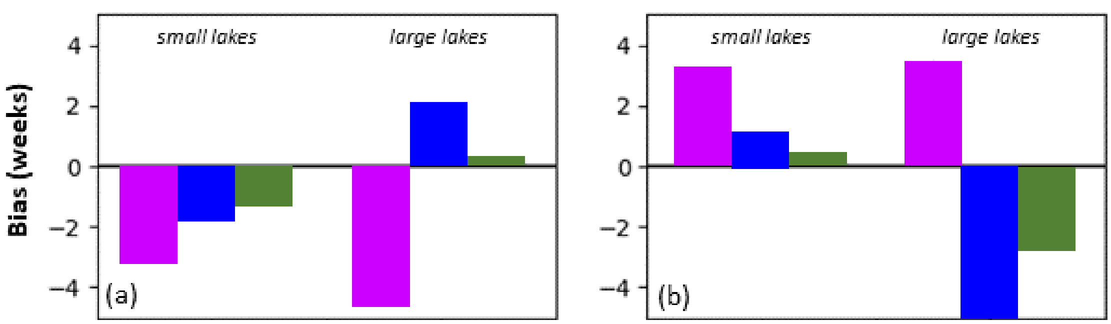

Fig. 3 Simulated bias in: (a) – ice-on; (b) – ice cover duration, based on 2016 – 2018 weekly Canadian Ice Service data for 115 lakes. Results are separated based on lake area where “small” (96 lakes) and “large” (19 lakes) refers to areas less than or greater than 2000 km^2. Results for no ice mechanics (magenta), plastic failure (P^* = 27.5 kPa, blue), and viscoelastic buckling failure (green) are shown.

4 Discussion

By employing the elastic – viscoelastic correspondence principle from the theory of continuum mechanics we have derived a general condition for the linear viscoelastic buckling of ice and applied it to the Maxwell rheological model – the simplest model that includes secondary creep. There are of course many other models (infinitely many) to choose from. For example, the simplest model that includes primary creep (*i.e.* delayed elasticity) is the Kelvin (Voigt) model, given by $\hat{\boldsymbol{P}}(\boldsymbol{s}) = \mathbf{1}$; $\hat{\boldsymbol{Q}}(\boldsymbol{s}) = \boldsymbol{E} + \boldsymbol{\eta s}$. Repeating the above analysis with this model yields an expression identical to (11) except the expression in the curly brackets becomes the error function $\mathbf{erf}\left(\sqrt{\frac{\boldsymbol{E}}{\boldsymbol{\eta}}}\sqrt{\boldsymbol{t}}\right)$ whose maximum value is 1. Thus the impact of delayed elasticity is merely to delay the elastic buckling that would have taken place in the absence of viscosity, and is thus inappropriate for our purposes (though again may have other applications). More complex models can be constructed from groups of Maxwell and Kelvin units connected in series and/or parallel should sufficient data exist to estimate the additional material constants; however, a simple Maxwell model seems sufficient to represent the limited data we have shown in Fig. 1, and to achieve improved results with respect to CIS observed ice phenology (Figs. 2, 3). Also, an appealing feature of (11) is that it is analytic; more complex rheological models would almost certainly require numerical inverse Laplace transforms.

In the above analysis we have neglected any temporal evolution in Poisson's ratio ν, regarding it as a fixed parameter with a nominal value of 0.3. Strictly speaking, both E and ν are represented by differential operators in viscoelastic analysis, frequently with different sets of operators (different rheological models) representing the dilatational and deviatoric components of the deformation (*e.g.* Findley et al., 1989). The above analysis can be repeated for this more general case, but the physical meaning becomes somewhat obscured, and again we will almost certainly require numerical inverse Laplace transforms.

Finally, we have pointed out that the Maxwell model reduces to the purely elastic case in the limit $\boldsymbol{\eta} \to \infty$ in which case (11) reduces to (6). At the other extreme, in the limit $\boldsymbol{E} \to \infty$ the Maxwell model reduces to a purely viscous fluid. The creep buckling of a viscous plate has been analyzed by Staroszczyk and Hedzielski (2004) and Sjolind (1985) and it is important to understand our results in the context of these earlier studies. The analogue of elastic buckling for a viscous plate can be analyzed exactly as above starting with (7) but taking as the rheological model

$$\widehat{\boldsymbol{P}}(\boldsymbol{s}) = \mathbf{1};\ \widehat{\boldsymbol{Q}}(\boldsymbol{s}) = \boldsymbol{\eta s}$$

which is a Maxwell fluid in the limit $\boldsymbol{E} \to \infty$. The final temporal dependence is different (proportional to $\sqrt{\boldsymbol{t}}$) but a similar curve to that shown in Fig. 1 for viscoelastic buckling is easily generated with judicious parameter selection. However the instability described here is not the same as the amplification of finite amplitude disturbances discussed in these previous studies. Buckling represents a bifurcation in the solution to a governing linear differential equation. At the point of bifurcation an infinitesimal perturbation will transition the system from an unbuckled to an infinitesimally close by buckled state, after a time delay between the application of stress and the initiation of buckling. During this period, deformation occurs and the elastic constants evolve until the buckling condition is met. Post-buckling amplification and failure is not explicitly modeled but assumed to occur in short order. In the creep buckling studies of Staroszczyk and Hedzielski (2004) and Sjolind (1985) small but finite initial disturbances grow to large amplitude after a few hours assuming the initial linear governing equation remains valid. Neither approach completely solves the problem; to do so requires a nonlinear, large amplitude theory.

5 Conclusions

In this study a simple lake ice concentration scaling law is proposed based on a linear viscoelastic stability analysis of thin ice sheets under low stress conditions at geophysical scales. The addition of viscosity to the constitutive equation has two important impacts relevant to our goal. First, it introduces a time dependence to the deformation and failure of ice that is significant on synoptic timescales; in particular the apparent rigidity of the ice decreases sufficiently over a few hours so that much thicker ice cover can buckle compared with the purely elastic case. In addition the time history of the wind forcing becomes relevant so that the impact of for example a series of wind events accumulates leading to failure that might not occur for the elastic case. The viscoelastic analysis presented here includes both purely elastic and purely viscous ice cover as special cases, though we have emphasized that the viscous creep buckles of some previous studies result from a different process.

Based on multiannual simulations over Canada and the northern U.S. we find that ice phenology is generally improved with the proposed viscoelastic mechanism compared with plastic failure, and greatly improved compared with the case of no ice mechanics.

Acknowledgments

Code development, implementation and testing of the Canadian Small Lake Model within the Surface Prediction System was greatly facilitated by the efforts of Maria Abrahamowicz, Étienne Gaborit, Camille Garnaud, Vivian Lee, and Katja Winger. Ice concentration and thickness data were provided by the Canadian Ice Service. Helpful comments on the manuscript by Jean-François Lemieux are gratefully acknowledged.

Open Research

Data Availability Statement

All simulation and observed data, as well as analysis and plotting programs used in this study are available at zenodo via https://doi.org/10.5281/zenodo.7743224 (MacKay, 2023). Observed ice concentration and thickness data are also available from the Canadian Ice Service by emailing cisclients-scgclients@ec.gc.ca. Figures were produced with Matplotlib, available at https://matplotlib.org. Laplace transforms were computed online with Wolfram|Alpha (https://www.wolframalpha.com).

References

Alfrey, T. (1944). Nonhomogeneous stress in viscoelasticity. *Quarterly of Applied Mathematics, 2(2)*, 113-119.

Balsamo, G., Salgado, R., Dutra, E., Boussetta, S., Stockdale, T., & Potes, M. (2012). On the contribution of lakes in predicting near –surface temperature in a global weather forecasting model. *Tellus A, 64,* 15829. https://doi.org/10.3402/tellusa.v64i0.15829

Biot, M. A. (1954). Theory of stress – strain relations in anisotropic viscoelasticity and relaxation phenomena. *Journal of Applied Physics*, *25*, 1385-1391.

Biot, M. A. (1965). *Mechanics of Incremental Deformations*. New York, NY: John Wiley and Sons Inc.

Durnford, D., Fortin, V., Smith, G., Archambault, B., Deacu, D., Dupont, F., Dyck, S., Martinez, Y., Klyszejko, E., MacKay, M., Liu, L., Pellerin, P., Pietroniro, A., Roy, F., Vu, V., Winter, B., Yu, W., Spence, C., Bruxer, J., & Dicjhout, J. (2018). Toward an operational water cycle prediction system for the Great Lakes and St. Lawrence River. *Bulletin of the American Meteorological Society*, *99*, 521-546. https://doi.org/10.1175/BAMS-D-16-0155.1

Eerola, K., Rontu, L., Kourzeneva, E., Kheyrollah Pour, H., & Duguay, C. (2014). Impact of a partly ice-free Lake Ladoga on temperature and cloudiness in an anticyclonic winter situation – a case study using a limited area model. *Tellus A, 66*, 23929. https://doi.org/10.3402/tellusa.v66.23929

Findley, W. N., Lai, J. S., & Onaran, K. (1989). *Creep and Relaxation of Nonlinear Viscoelastic Materials*, New York, NY: Dover Publications.

Flügge, W. (ed). (1962). *Handbook of Engineering Mechanics*. New York, NY: McGraw – Hill.

Gammon P., Kiefte, H., Clouter, M., & Denner, W. (1983). Elastic constants of artificial and natural ice samples by Brillouin spectroscopy. *Journal of Glaciology, 29*, 433-460.

Gasset, N., Fortin, V., Dimitrijevic, M., Carrera, M., Bilodeau, B., Muncaster, R., Gaborit, E., Roy, G., Pentcheva, N., Bulat, M., Wang, X., Pavlovic, R., Lespinas, F., Khedhaouiria, D., & Mai, J. (2021). A 10 km North American precipitation and land-surface reanalysis based on the GEM atmospheric model. *Hydrology and Earth System Sciences*, *25*, 4917-4945. https://doi.org/10.5194/hess-25-4917-2021

Garnaud, C., MacKay, M., & Fortin, F. (2022). A one-dimensional lake model in ECCC's land surface prediction system. *Journal of Advances in Modeling Earth Systems, 14,* e2021MS002861. https://doi.org/10.1029/2021MS002861

Hetényi, M. (1946). Beams on elastic foundation. *University of Michigan Studies Scientific Series*, XVI, Ann Arbor, MI: The University of Michigan Press.

Hibler, W. D. III. (1979). A dynamic thermodynamic sea ice model. *Journal of Physical Oceanography, 9,* 815-846.

Hibler, W. D. III, & Walsh, J. (1982). On modeling seasonal and interannual fluctuations of Arctic sea ice. *Journal of Physical Oceanography, 92*, 1514-1523.

Hopkins, M. (1998). Four stages of pressure ridging. *Journal of Geophysical Research*, *103*, C10, 21883-21891.

Kirillin, G., Leppäranta, M., Terzhevik, A., Granin, N., Bernhardt, J., Engelhardt, C., Efremova, T., Golosov, S., Palshin, N., Sherstyanki, P., Zdorovennova, G., & Zdorovennov, R. (2012). Physics of seasonally ice-covered lakes: a review. *Aquatic Sciences, 74,* 659-682. https://doi.org/10.1007/s00027-012-0279-y

Le Moigne, P., Colin, J., & Decharme, B. (2016). Impact of lake surface temperatures simulated by the FLake scheme in the CNRM-CM5 climate model. *Tellus A, 68,* 31274. https://doi.org/10.3402/tellusa.v68.31274

Lee, E. H. (1955). Stress analysis in viscoelastic bodies. *Quarterly of Applied Mathematics,* ***13***, 183-190.

Leppäranta, M., & Wang, K. (2008). The ice cover on small and large lakes: scaling analysis and mathematical modelling. *Hydrobiologia*, *599*, 183-189. https://doi.org/10.1007/s10750-007-9201-3

MacKay, M. (2023). Ice Mechanics for 1-D Lake Models [Dataset]. Zenodo. https://doi.org/10.5281/zenodo.7743224

Mironov, D., Heise, E., Kourzeneva, E., & Terzhevik, A. (2010). Implementation of the lake parameterization scheme FLake into the numerical weather prediction model COSMO. *Boreal Environment Research,* 15, 218-230.

Parmerter, R. (1974). Dimensionless strength parameters for floating ice sheets. *AIDJEX Bulletin,* 23, 83-95.

Parmerter, R. (1975). A model of simple rafting in sea ice. *Journal of Geophysical Research,* 80, 1948-1952.

Parmerter, R., & Coon, M. (1972). Model of pressure ridge formation in sea ice. *Journal of Geophysical Research,* 77, 6565-6575.

Pietikäinen, J.-P., Markkanen, T., Sieck, K., Jacob, D., Korhonen, J., Räisänen, P., Gao, Y., Ahola, J., Korhonen, H., Laaksonen, A., & Kaurola, J. (2018). The regional climate model REMO (v2015) coupled with the 1-D freshwater lake model FLake (v1): Fenno-Scandinavian climate and lakes. *Geoscientific Model Development, 11,* 1321-1342. https://doi.org/10.5194/gmd-11-1321-2018

Rontu, L., Eerola, K., & Horttanainen, M. (2019). Validation of lake surface state in the HIRLAM v.7.4 numerical weather prediction model against in situ measurements in Finland. *Geoscientific Model Development, 12,* 3707-3723. https://doi.org/10.5194/gmd-12-3707-2019

Rothrock, D. A. (1975). The steady drift of an incompressible Arctic ice cover. *Journal of Geophysical Research, 80,* 387-397.

Schulson, E. (2004). Compressive shear faults within Arctic sea ice: fracture on scales large and small. *Journal of Geophysical Research, 109*, C07016. https://doi.org/10.1029/2003JC002108

Sjolind, S.-G. (1985). Viscoelastic buckling analysis of floating ice sheets. *Cold Regions Science and Technology, 11,* 241-246.

Staroszczyk, R. & Hedzielski, B. (2004). Creep buckling of a wedge-shaped floating ice plate. *Engineering Transactions*, *52,* 111-130.

Subin, Z., Riley, W., & Mironov, D. (2012). An improved lake model for climate simulations: Model structure, evaluation, and sensitivity analyses in CESM1. *Journal of Advances in Modeling Earth Systems*, *4,* M02001. https://doi.org/10.1029/2011MS000072

Verseghy, D. (2017). CLASS – The Canadian Land Surface Scheme (version 3.6.1). Technical Documentation, Environment and Climate Change Canada.

Ice Concentration Scaling Laws for Freshwater Lakes in Numerical Weather and Climate Prediction

Murray D. MacKay[1]

[1]Meteorological Research Division, Environment and Climate Change Canada, Toronto, Canada

Corresponding author: Murray MacKay (murray.mackay@ec.gc.ca)

Key Points:

- Most one-dimensional lake models neglect ice mechanics or assume plastic failure, and frequently perform poorly regarding ice phenology.
- Assuming lake ice fails as a linear viscoelastic material at geophysical scales leads to a simple parameterization of ice concentration.
- The new scheme outperforms plastic failure or the absence of mechanics with respect to ice – on and ice duration.

Abstract

If lake ice is assumed to deform and fail as a linear viscoelastic material under the action of wind stress, then a simple ice concentration scaling law can be constructed suitable for one-dimensional lake models embedded within environmental prediction systems. Most 1-D lake models assume no ice mechanics at all, while others adapt the viscous-plastic rheology common in ice-ocean models for the purpose of estimating ice fraction. Elastic buckling is generally disregarded as a significant failure mechanism in ice under low stress conditions at geophysical scales. However, by adding viscosity to the constitutive equation, the conditions for viscoelastic buckling seem quite plausible over a wide range of lake size and ice thickness. An ice concentration scaling law based on this process is evaluated here in multiannual simulations over North America and found to produce superior ice phenology statistics compared with simulations based on plastic failure or no ice mechanics.

Plain Language Summary

Most mid- and high- latitude lakes experience periods of partial ice cover (*i.e.* ice concentration < 100%) during early winter. While very small lakes might freeze solid in a single night under calm conditions, larger lakes may take days or weeks to completely freeze because wind stress continually breaks the ice cover resulting in patches of open water. The extent of wintertime open water is very important for both lake ecology and for regional weather conditions (*e.g.* lake-effect snowstorms). Many weather and climate models employ one-dimensional lake models that do not represent fractional ice cover at all, or parameterize it based on mechanical ideas from sea ice models, resulting in poor timing and duration of simulated ice cover. Here we propose a new scheme based on different mechanics that improves these simulated features.

1 Introduction

The interface between a lake and the overlying atmosphere regulates flux exchange between the two, and the state of ice at the lake surface – both in terms of thickness and concentration (*i.e.* fractional cover) – is the predominant governing factor for much of the year in high- and mid-latitude regions. Areas of thick ice, especially if snow covered, severely restrict the transmission of shortwave radiation and gas exchange with obvious impacts on lake ecology.

On the other hand many lakes experience only partial ice cover for much (if not all) of the winter, and patches of open water can lead to for example surface oxygen renewal and nutrient redistribution (through circulation) and increased primary production (through increased light penetration), not to mention major fluxes of heat and moisture into the generally cold, dry air above. It is clear that climate and numerical weather prediction modelling systems that incorporate some representation of lakes need to consider the nature of lake ice carefully, especially under conditions of fractional cover. For modelling systems that employ 3-dimensional lake models with fully dynamic ice schemes (*e.g.* Durnford et al., 2018) this is generally not a problem. However, many forecasting systems represent lakes with simple one-dimensional thermodynamic models, for which ice mechanics must be parameterized in order to simulate the correct balance of ice cover and open water.

One – dimensional lake schemes have been used in a number of short-range forecasting studies that examined ice conditions (*eg.* Rontu et al., 2019; Eerola et al., 2014; Balsamo et al., 2012). In all of these studies ice-on tended to occur too early, at least partially due to the fact that the lake scheme employed (FLake – Mironov et al., 2010) did not represent fractional ice cover. In this scheme, once ice grows to a thickness of 1 mm it is assumed to cover the entire lake (or gridcell for large lakes). In reality such ice is easily broken by wind or waves and rafted, resulting in both open water and ice-covered areas. However, the period of partial ice cover may be short lived for small lakes and larger lakes could benefit from data assimilation – at least for short range forecasts.

The situation is more problematic for long range forecasts and climate simulations. In a climate modelling study over Northern Europe based on the Max Plank Institute’s REMO coupled with FLake, Pietikäinen et al. (2018) found ice-on dates were again too early: 2-3 weeks for moderately sized (100 – 1000 km^2) Finnish lakes, but more than 1 month early for Lakes Vättern (1912 km^2) and Onega (9700 km^2) and more than 2 months early for Lake Ladoga (17,700 km^2). In Le Moigne et al. (2016), ice-on is not evaluated *per se* though the authors discuss the necessity of setting ice and snow albedos arbitrarily low in FLake in order to account for radiative impacts of fractional ice cover. This issue was also noted by Subin et al. (2012) for the Lake, Ice, Snow, and Sediment Simulator (LISSS), a one – dimensional lake model that also neglects fractional ice cover. In addition, while ice-on dates were not evaluated extensively, this study did note that ice-on occurred several weeks too early for their simulation of Great Slave Lake.

Below we propose a simple approach to represent ice concentration in any 1-dimensional lake model. The key ingredient is the determination of a critical ice thickness above which ice concentration tends to remain stable at 100%. Below this thickness ice is assumed to break and ridge or raft, resulting in the presence of some open water.

2 A Universal Scaling Law for Critical Lake Ice Thickness?

Open water leads in ice cover (for both lakes and oceans) are frequently generated under the action of wind stress that mechanically breaks sufficiently thin ice and forces the rubble into ridges (*e.g.* Hopkins, 1998) a process that has been successfully represented in a modelling study of Lake Peipsi by Leppäranta and Wang (2008). Following Hibler (1979), Leppäranta and Wang view ice as a viscous-plastic medium with a yield strength given by

$$P = P^{*}h\, exp\{-C(1-A)\} \qquad (1),$$

where h is the mean ice thickness, A is the ice compactness, C is a strength reduction factor, and P^* is the compressive strength of compact ice (per unit thickness). Leppäranta and Wang (2008) suggest these last two parameters be >>1 and 10-100 kPa respectively. When fully compact (*i.e.* A=1) the ice will break due to wind stress τ_a when

$$h < H = \left(\frac{\tau_a}{P^*}\right) L \qquad (2),$$

where L is taken as the fetch over the lake. When ice thickness is greater than this critical threshold it is considered stable; when it is thinner it breaks and forms pressure ridges and open water leads. An order of magnitude argument suggests that for wind stress ~ 0.15 Pa and P^* = 27.5 kPa (*e.g.* Hibler & Walsh, 1982) we get $H \approx 5.4\, x10^{-6} L$. Thus for Lake Peipsi with a mean fetch of about 50 km, Leppäranta and Wang (2008) find that ice is “movable” (*i.e.* subject to mechanical breakup and ridging) when it is thinner than about 27 cm, and stable when it is thicker, in agreement with observations.

At first glance this relationship between critical ice thickness H and fetch L may seem reasonable as larger ice fields would sustain more wind stress and thus require greater thickness to be mechanically stable. However (2) clearly fails for very large lakes. Great Bear and Great Slave lakes in northern Canada have mean fetch on the order of 170 km, yet both lakes routinely freeze solid with ice thicknesses of only 55 – 65 cm, whereas (2) implies 93 cm. Leppäranta and Wang (2008) (see also Kirillin et al., 2012) emphasized that $P*$ could be tuned based on data. However, tuning (2) for Great Bear and Great Slave lakes degrades results for Lake Peipsi (see below).

A scaling law based on (2), however, is not the only choice. For example, if elastic buckling was deemed important prior to ridging then the strength of ice (e.g. Parmerter, 1974) is given by

$$P = \left(\frac{E\rho_w g H^3}{12(1-\upsilon^2)}\right)^{1/2} \qquad (3),$$

where E and ν are the Young's modulus and Poisson's ratio for ice, ρ_w is the density of water, and g is the acceleration due to gravity. This follows from treating the ice cover as a thin plate floating on an elastic (*i.e.* Winkler) foundation (Hetenyi, 1946). Because this would lead to ice much stronger than (2), Rothrock (1975) appears to rule out elastic buckling as an important mechanism in ridging, a sentiment echoed in Schulson (2004).

Other studies have retained the buckling process, though there has been considerable latitude with respect to the value of the Young's modulus selected. Parmerter (1974, 1975) found that 0.3 GPa gave good results in a study of sea ice rafting. Hopkins (1998) chose E = 0.1 GPa in order to achieve reasonable results in an ice ridging model. On the other hand Parmerter and Coon (1972) found that E = 1 GPa worked well for their ridging model.

Now from (3) we find that

$$L\tau_a = \left(\frac{E\rho_w g H^3}{12(1-\upsilon^2)}\right)^{\frac{1}{2}} \qquad (4)$$

becomes

$$H = \left[\frac{\tau_a}{\alpha E^{1/2}}\right]^{2/3} L^{2/3} \qquad (5)$$

where

$$\alpha = \left[\frac{\rho_w g}{12(1-\nu^2)}\right]^{1/2} = 29.96\ [\mathrm{Pa}^{1/2} m^{-1/2}]$$

assuming ν = 0.3 (Gammon et al., 1983).

There are scant relevant observed data to verify these scaling laws for a critical ice thickness over lakes, primarily because of the difficulty in safely measuring ice thickness under conditions of incomplete or marginally complete ice cover. Somewhat fortuitously, the Canadian Ice Service (CIS), has observed weekly ice concentration data from over 100 North American lakes since about 1995, and weekly ice thickness data from two measurement programs (1947-2002; 2002-2020) over a few lake and ocean locations. All three programs are independent and served different objectives, though there is some overlap for three important lakes – Great Bear Lake (31,153 km^2), Great Slave Lake (27,200 km^2) and Baker Lake (1887 km^2), which we have plotted in Fig. 1.

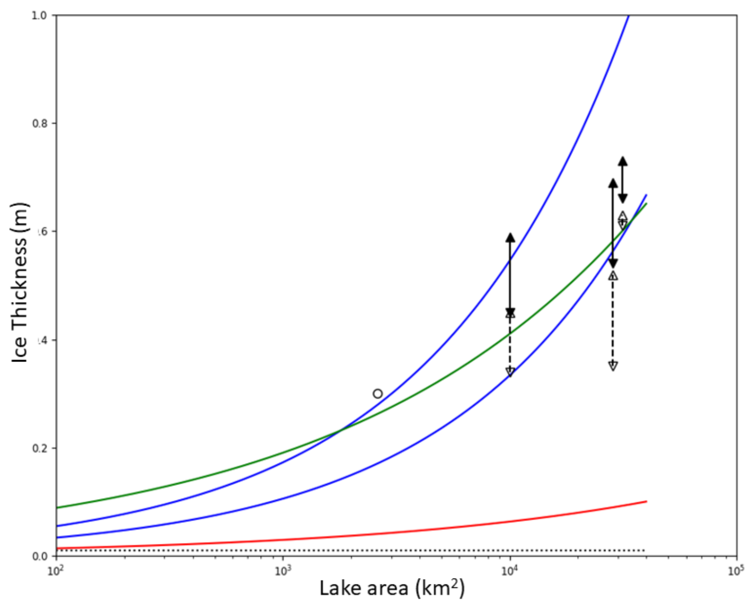

Fig. 1 Critical ice thickness as a function of lake area. Black vertical lines and symbols represent observed estimates. Blue curves represent plastic failure (2) with *P** = 27.5 kPa (upper curve) and *P** = 45 kPa (lower curve). Red curve represents elastic buckling failure (5) with *E* = 1 GPa. Green curve represents viscoelastic buckling failure (11) with *E* = 9.0 GPa, $\eta = 10^{11}$ $kg\ m^{-1} s^{-1}$, and assuming steady wind forcing for 6 hours. All solid curves assume wind stress ~ 0.15 Pa. Fetch is estimated as the square root of lake area. The dotted horizontal black line represents a threshold of 1.0 cm for complete ice cover (*i.e.* no ice mechanics). See text for details.

In this figure, solid vertical black lines ending with filled triangles represent the interquartile range of ice thickness when ice concentration was first recorded as 100% (Great Bear Lake: n=4; Great Slave Lake: n=14; Baker Lake: n=16). The vertical black dashed lines ending with unfilled triangles represent the interquartile range of ice thickness when ice concentration was last recorded as 90% (Great Bear Lake: n=4; Great Slave Lake: n=12; Baker Lake: n=15). Thus we estimate that the average critical ice thickness when these lakes first reached 100% ice cover is approximately midway between these solid and dashed segments. Lake Peipsi (2611 km^2) is also indicated in Fig. 1 (open circle) near the point of marginally complete ice cover. Note that in this figure mean lake fetch L is estimated as the square root of lake area, with the exception of Baker lake which is highly elongated in the east-west direction, roughly 100 km in extent.

Fig. 1 also shows the scaling models described above. The blue curves show (2) with: $P*$ = 27.5 kPa (upper curve), and $P*$ = 45 kPa (lower curve). Neither curve is consistent with all of the observed data presented. Elastic buckling failure (5) is represented by the red curve. Even assuming the Young's modulus as low as E = 1 GPa, the ice is still much stronger than the observed data suggest.

2.1 The Viscoelastic Buckling of Lake Ice

The condition for classical elastic buckling of a floating thin plate (3) due to some axial force F can be written

$$\left(\frac{\rho_w g H^3}{12(1-\upsilon^2)}\right)^{1/2} E^{1/2} = F. \qquad \textbf{(6)}$$

Classical buckling is generally understood as a bifurcation in the equilibrium condition of the structure in question, where the buckled solution is infinitesimally close to the unbuckled solution (*e.g.* Flügge, 1962, ch. 44). Buckling in and of itself does not necessarily imply *failure* – in our context the actual breakage and ridging or rafting of ice – though this is generally tacitly assumed for thin sheets of ice. A rigorous post-bucking analysis would require a nonlinear finite amplitude theory (*e.g.* Biot, 1965), beyond the scope of this study. As a first step here we extend the linearized, small amplitude stability analysis of thin elastic (floating) sheets of ice into the viscoelastic realm and assume failure to occur shortly after the conditions for buckling are met.

The generalization of elasticity theory to viscoelastic materials can be achieved for a large class of problems by way of a *correspondence principle*, first elucidated by Alfrey (1944), Biot (1954), and Lee (1955). In viscoelasticity, the constitutive equations are generalized based on linear differential operators (P(t), Q(t)) of the rheological model selected, introducing a time dependence to the governing equations. It has long been recognized that taking the Laplace transform of the viscoelastic equations renders a set of equations in transform space formally identical to a corresponding elastic problem if E in the elastic system is replaced by $\hat{Q}(s)/\hat{P}(s)$ in the transformed problem where $\hat{Q}, \hat{P}$ are the Laplace transforms of Q, P respectively. To solve the viscoelastic problem one simply needs to compute the inverse Laplace transform once this substitution is made.

Thus in Laplace transform space, the condition for viscoelastic instability corresponding to (6) becomes

$$\left(\frac{\rho_w g H^3}{12(1-\upsilon^2)}\right)^{1/2}\left(\frac{\hat{Q}(s)}{\hat{P}(s)}\right)^{1/2} = \hat{F}(s) \qquad \textbf{(7)}$$

where $\hat{F}(s)$ is the Laplace transform of the wind forcing F(t), now in general a function of time. This can be solved by inverse Laplace transform once a suitable rheological model is selected. A simple choice that includes both elastic and creep deformation is the Maxwell fluid, represented by

$$\hat{P}(s) = 1 + \frac{\eta}{E}s; \qquad \hat{Q}(s) = \eta s,$$

where η is a viscosity. Now (**7**) becomes

$$\left(\frac{\rho_w g H^3}{12(1-\upsilon^2)}\right)^{1/2} = \frac{1}{\sqrt{\eta}}\hat{F}(s)\hat{G}(s)\ , \qquad \textbf{(8)}$$

where

$$\hat{G}(s) = \left(\frac{1+\frac{\eta}{E}s}{s}\right)^{1/2}$$

has the inverse Laplace transform

$$G(t) = \frac{1}{2}\left(\frac{E}{\eta}\right)^{1/2} \exp\left(-\frac{1}{2}\frac{E}{\eta}t\right)\left[I_0\left(\frac{1}{2}\frac{E}{\eta}t\right) + I_1\left(\frac{1}{2}\frac{E}{\eta}t\right)\right] \qquad ;\ t>0. \quad \textbf{(9)}$$

where I_0 and I_1 are modified Bessel functions of the first kind. It is important to notice that (9) is valid only for t>0; the case for t=0 must be handled separately and added. It is clear on physical grounds that for t=0 we expect to recover the purely elastic case. For now we must add an unknown function G_0 to the RHS of (9), evaluated below, to solve over the full time domain.

By the convolution theorem of Laplace transforms, (8) with (9) becomes after inversion

$$\left(\frac{\rho_w g H^3}{12(1-\upsilon^2)}\right)^{1/2} = \frac{1}{\sqrt{\eta}}\left\{\int_{0^+}^{t} F(t-\tau)G(\tau)\,d\tau + G_0\right\}$$

$$= \frac{\sqrt{E}}{2\eta}\int_{0^+}^{t} F(t-\tau)\exp\left(-\frac{1}{2}\frac{E}{\eta}\tau\right)\left[I_0\left(\frac{1}{2}\frac{E}{\eta}\tau\right) + I_1\left(\frac{1}{2}\frac{E}{\eta}\tau\right)\right]d\tau + \frac{G_0}{\sqrt{\eta}}\,. \qquad \textbf{(10)}$$

This represents the general condition for linear viscoelastic buckling of a Maxwell material under some time dependent wind forcing F(t). Notice that both the material constants E, η, as well as the time history of the forcing are relevant to the buckling criterion. This distinguishes it from the purely elastic case which is instantaneous - it either buckles or it doesn't – depending on E, and the instantaneous magnitude (not the time history) of the applied force.

Consider now the case of a steady wind stress applied at t=0, so that

$$F(t) = L\tau_a \mathcal{H}(t)$$

where $\mathcal{H}(t)$ is the unit Heaviside function. For this case (10) becomes

$$\left(\frac{\rho_w g H^3}{12(1-\upsilon^2)}\right)^{\frac{1}{2}} = L\tau_a \frac{\sqrt{E}}{2\eta}\int_0^t \exp\left(-\frac{1}{2}\frac{E}{\eta}\tau\right)\left[I_0\left(\frac{1}{2}\frac{E}{\eta}\tau\right) + I_1\left(\frac{1}{2}\frac{E}{\eta}\tau\right)\right]d\tau + \frac{G_0}{\sqrt{\eta}}$$

$$= \frac{L\tau_a}{\sqrt{E}}\left\{-1 + \exp\left(-\frac{1}{2}\frac{E}{\eta}t\right)\left[\left(\frac{E}{\eta}t + 1\right)I_0\left(\frac{1}{2}\frac{E}{\eta}t\right) + \left(\frac{E}{\eta}t\right)I_1\left(\frac{1}{2}\frac{E}{\eta}t\right)\right]\right\} + \frac{G_0}{\sqrt{\eta}}$$

It is clear that if we select $G_0 = L\tau_a\sqrt{\frac{\eta}{E}}$ then this becomes

$$\left(\frac{E\rho_w g H^3}{12(1-\upsilon^2)}\right)^{\frac{1}{2}} = L\tau_a\left\{\exp\left(-\frac{1}{2}\frac{E}{\eta}t\right)\left[\left(\frac{E}{\eta}t + 1\right)I_0\left(\frac{1}{2}\frac{E}{\eta}t\right) + \left(\frac{E}{\eta}t\right)I_1\left(\frac{1}{2}\frac{E}{\eta}t\right)\right]\right\} \quad \textbf{(11)}$$

which reduces to the elastic buckling condition (6) for t=0 as required. Note that for the Maxwell model the elastic limit is also recovered for $\eta \rightarrow \infty$, so we consider (11) the viscoelastic generalization of (6) for the Maxwell model under steady wind forcing. For finite values of η but on short timescales, series expansions of the exponential and modified Bessel functions suggest

$$\left(\frac{E\rho_w g H^3}{12(1-\upsilon^2)}\right)^{\frac{1}{2}} \approx L\tau_a\left\{1 + \frac{1}{2}\frac{E}{\eta}t\right\}; \quad \frac{E}{\eta}t \ll 1$$

Taking E = 9.0 GPa and $\eta = 10^{11}$ $kg\ m^{-1}s^{-1}$ (*e.g.* Staroszczyk & Hedzielski, 2004) this approximation requires t << 22 s. Thus for wind forcing on synoptic timescales this condition, which could be called *nearly elastic* bucking, does not seem relevant, though it may be appropriate for other types of linear viscoelastic problems (*e.g.* slowly colliding ice plates). If we consider a steady wind stress (0.15 Pa) acting on the ice field for 6 hours, then the term in the curly brackets in (11) evaluates to 49.75. This is represented by the green curve in Fig. 1 which fits the data much better than the other models. Note we do not require a full 6 hours of steady wind to achieve buckling here. The linear form of (10) indicates that a series of shorter but stronger wind gusts would achieve the same thing. This is clear if F in (10) is replaced with a series of pulses represented by positive and negative Heaviside step functions, perhaps of different amplitudes.

Ice thickness data near the time of freeze-up are difficult to come by. On the other hand, ice concentration data are much more readily available, which we can relate to ice failure through numerical simulation. In the following section we discuss a series of simulations that parameterize ice mechanics based on (2) or (11) described above, as well as the absence of mechanics. As will become clear, the impact of these schemes on fractional ice cover is dramatic. We evaluate these simulations based on Canadian Ice Service observed ice concentration data from 115 lakes over North America in order to help select the optimal approach.

3 Simulations

Recently Garnaud et al. (2022) described simulations of Environment and Climate Change Canada's Surface Prediction System (SPS), which had incorporated a one – dimensional thermodynamic lake scheme. Ice mechanics was parameterized following (2) above, *i.e.* when $\boldsymbol{h} \geq \boldsymbol{H}$ the ice cover was considered complete (fractional ice cover F_{ice} = 1.0), and when $\boldsymbol{h} < \boldsymbol{H}$ the fractional ice cover was computed as $F_{ice} = h/H$. This simple linear approach has been used to parameterize, for example, fractional snow cover in the Canadian Land Surface Scheme (CLASS) for many years (*e.g.* Verseghy, 2017). The compressive strength of ice P^* was set to 27.5 kPa, as in Leppäranta and Wang (2008). Simulations ran on a 2.5 km horizontal resolution grid covering most of Canada and the northern U.S.A. from 1 September 2015 – 31 December 2018. It was found that the new lake scheme improved ice phenology for the smallest lakes, compared with the existing approach (which was largely based on data assimilation), but that this improvement degraded as lake surface area increased. In terms of ice mechanics this behavior could be anticipated from our Fig. 1 (upper blue curve) where it is clear that (2) will produce fractional ice cover for the largest lakes when observations suggest that ice cover is complete (see also below).

Here we perform an identical simulation to that of Garnaud et al. (2022), except we drive SPS with a slightly improved atmospheric and precipitation forcing data set (Gasset et al., 2021).

In addition to parameterizing ice mechanics based on plastic failure (2), we also include simulations based on viscoelastic buckling failure (11), and by assuming no mechanics at all. This last criterion is achieved by setting ice concentration to 100% when ice thickness reaches 1.0 cm (Fig. 1 black dotted curve), similar to the approach used in FLake as noted above.

Ice concentration from all 3 simulations is evaluated against observations from the CIS, examples of which are illustrated in Fig. 2. Fig. 2a shows weekly results for Great Bear Lake, the largest lake in the data set at 31,153 km^2. For each of the 3 winter periods examined, ice-on is clearly too early in the simulation without mechanics (magenta crosses), and too late (or absent) in the simulation assuming plastic failure (blue circles), while the simulation assuming viscoelastic mechanics is better in this respect (green diamonds). For La Grande Reservoir (Fig. 2b – 2835 km^2) ice – on is again several weeks too early in the simulation without mechanics, while the other simulations show nearly identical (and much better) results. Finally, Fig. 2c shows results for a smaller lake – Leech Lake (417 km^2). Ice – on in the simulation without mechanics is still too early. The other simulations are again similar, but examination of especially the 2017/18 winter reveals that ice – on is also too early in the simulation assuming plastic failure while it is better in the viscoelastic simulation. All of these results could have been anticipated from Fig. 1: the viscoelastic ice is harder than the plastic ice for lakes larger than about 2000 km^2 (green curve lies below the upper blue curve), and softer for lakes smaller

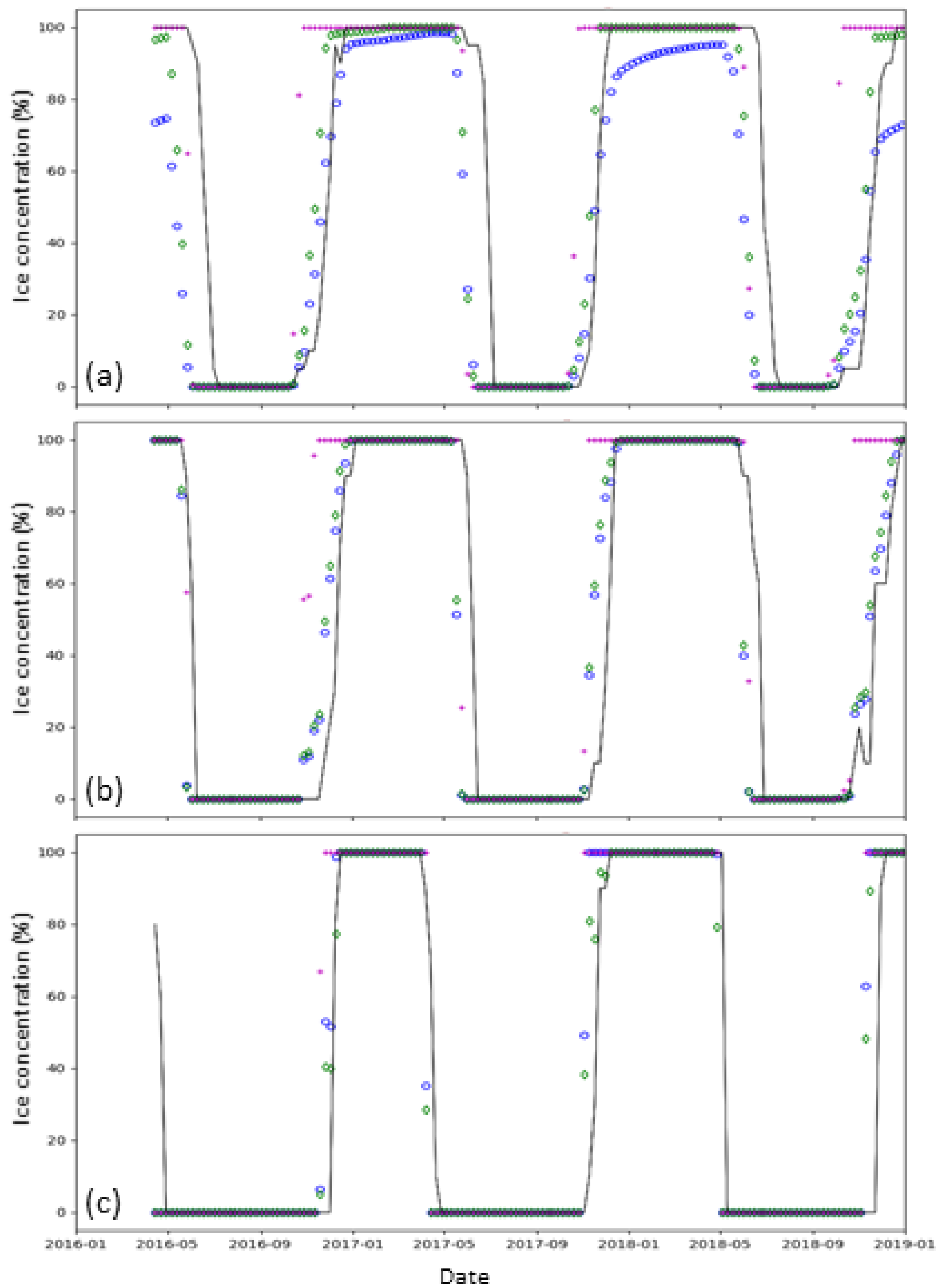

Fig. 2 Observed (thin black curves) and simulated ice concentration (January 2016 – January (2019) for: (a) - Great Bear Lake (31153 km^2); (b) - La Grande Reservoir (2835 km^2); and (c) – Leech Lake (417 km^2). Simulated values assume plastic failure with P^* = 27.5 kPa (blue circles); Viscoelastic buckling failure (green diamonds); and no mechanics (magenta crosses).

than 2000 km^2 (green curve lies above the upper blue curve). For lakes around 2000 km^2 in area both mechanical models produce similar results.

Fig. 3 summarizes ice phenology biases for all 115 lakes for which we have CIS data during this period. Results are separated based on lake size, as suggested above, where "small" refers to areas less than 2000 km^2 and "large" refers to lakes larger than this threshold. Based on this partition, the CIS data set contains 96 small and 19 large lakes. Because the CIS ice concentration observations are weekly and in units of tenths, ice – on (Fig. 3a) is defined as the first week of 90% ice cover, and ice cover duration (Fig. 3b) is defined as the number of weeks of ≥ 90% ice cover. On average the viscoelastic model outperforms the other simulations in both metrics for both small and large lakes: ice-on bias is only -8 days (small) and 1 day (large), compared with -12 days, 14 days (plastic), and -21 days, -32 days (no mechanics). Likewise, viscoelastic ice cover duration bias is only 3 days, -18 days (small, large) compared with 7 days, -34 days (plastic), and 22 days, 24 days (no mechanics). Note that none of the models handles the ice – off process particularly well (not shown). Differences due to the mechanics of melting, rotten, isothermal ice have not been considered here.

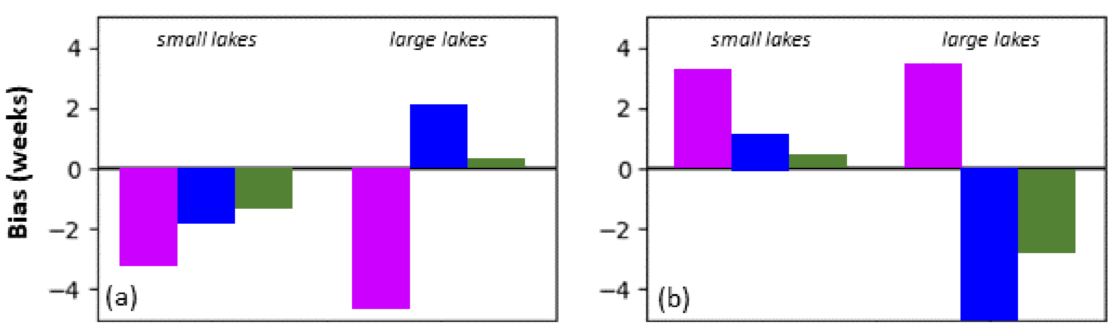

Fig. 3 Simulated bias in: (a) – ice-on; (b) – ice cover duration, based on 2016 – 2018 weekly Canadian Ice Service data for 115 lakes. Results are separated based on lake area where "small" (96 lakes) and "large" (19 lakes) refers to areas less than or greater than 2000 km^2. Results for no ice mechanics (magenta), plastic failure (P^* = 27.5 kPa, blue), and viscoelastic buckling failure (green) are shown.

4 Discussion

By employing the elastic – viscoelastic correspondence principle from the theory of continuum mechanics we have derived a general condition for the linear viscoelastic buckling of ice and applied it to the Maxwell rheological model – the simplest model that includes secondary creep. There are of course many other models (infinitely many) to choose from. For example, the simplest model that includes primary creep (*i.e.* delayed elasticity) is the Kelvin (Voigt) model, given by $\widehat{\boldsymbol{P}}(\boldsymbol{s}) = \mathbf{1}$; $\widehat{\boldsymbol{Q}}(\boldsymbol{s}) = \boldsymbol{E} + \boldsymbol{\eta s}$. Repeating the above analysis with this model yields an expression identical to (11) except the expression in the curly brackets becomes the error function $\mathbf{erf}\left(\sqrt{\frac{\boldsymbol{E}}{\boldsymbol{\eta}}}\sqrt{\boldsymbol{t}}\right)$ whose maximum value is 1. Thus the impact of delayed elasticity is merely to delay the elastic buckling that would have taken place in the absence of viscosity, and is thus inappropriate for our purposes (though again may have other applications). More complex models can be constructed from groups of Maxwell and Kelvin units connected in series and/or parallel should sufficient data exist to estimate the additional material constants; however, a simple Maxwell model seems sufficient to represent the limited data we have shown in Fig. 1, and to achieve improved results with respect to CIS observed ice phenology (Figs. 2, 3). Also, an appealing feature of (11) is that it is analytic; more complex rheological models would almost certainly require numerical inverse Laplace transforms.

In the above analysis we have neglected any temporal evolution in Poisson's ratio ν, regarding it as a fixed parameter with a nominal value of 0.3. Strictly speaking, both E and ν are represented by differential operators in viscoelastic analysis, frequently with different sets of operators (different rheological models) representing the dilatational and deviatoric components of the deformation (*e.g.* Findley et al., 1989). The above analysis can be repeated for this more general case, but the physical meaning becomes somewhat obscured, and again we will almost certainly require numerical inverse Laplace transforms.

Finally, we have pointed out that the Maxwell model reduces to the purely elastic case in the limit $\boldsymbol{\eta} \rightarrow \infty$ in which case (11) reduces to (6). At the other extreme, in the limit $\boldsymbol{E} \rightarrow \infty$ the Maxwell model reduces to a purely viscous fluid. The creep buckling of a viscous plate has been analyzed by Staroszczyk and Hedzielski (2004) and Sjolind (1985) and it is important to understand our results in the context of these earlier studies. The analogue of elastic buckling for a viscous plate can be analyzed exactly as above starting with (7) but taking as the rheological model

$$\hat{\boldsymbol{P}}(\boldsymbol{s}) = \mathbf{1};\ \hat{\boldsymbol{Q}}(\boldsymbol{s}) = \boldsymbol{\eta s}$$

which is a Maxwell fluid in the limit $\boldsymbol{E} \to \infty$. The final temporal dependence is different (proportional to $\sqrt{\boldsymbol{t}}$) but a similar curve to that shown in Fig. 1 for viscoelastic buckling is easily generated with judicious parameter selection. However the instability described here is not the same as the amplification of finite amplitude disturbances discussed in these previous studies. Buckling represents a bifurcation in the solution to a governing linear differential equation. At the point of bifurcation an infinitesimal perturbation will transition the system from an unbuckled to an infinitesimally close by buckled state, after a time delay between the application of stress and the initiation of buckling. During this period, deformation occurs and the elastic constants evolve until the buckling condition is met. Post-buckling amplification and failure is not explicitly modeled but assumed to occur in short order. In the creep buckling studies of Staroszczyk and Hedzielski (2004) and Sjolind (1985) small but finite initial disturbances grow to large amplitude after a few hours assuming the initial linear governing equation remains valid. Neither approach completely solves the problem; to do so requires a nonlinear, large amplitude theory.

5 Conclusions

In this study a simple lake ice concentration scaling law is proposed based on a linear viscoelastic stability analysis of thin ice sheets under low stress conditions at geophysical scales. The addition of viscosity to the constitutive equation has two important impacts relevant to our goal. First, it introduces a time dependence to the deformation and failure of ice that is significant on synoptic timescales; in particular the apparent rigidity of the ice decreases sufficiently over a few hours so that much thicker ice cover can buckle compared with the purely elastic case. In addition the time history of the wind forcing becomes relevant so that the impact of for example a series of wind events accumulates leading to failure that might not occur for the elastic case. The viscoelastic analysis presented here includes both purely elastic and purely viscous ice cover as special cases, though we have emphasized that the viscous creep buckles of some previous studies result from a different process.

Based on multiannual simulations over Canada and the northern U.S. we find that ice phenology is generally improved with the proposed viscoelastic mechanism compared with plastic failure, and greatly improved compared with the case of no ice mechanics.

Acknowledgments

Code development, implementation and testing of the Canadian Small Lake Model within the Surface Prediction System was greatly facilitated by the efforts of Maria Abrahamowicz, Étienne Gaborit, Camille Garnaud, Vivian Lee, and Katja Winger. Ice concentration and thickness data were provided by the Canadian Ice Service. Helpful comments on the manuscript by Jean-François Lemieux are gratefully acknowledged.

Open Research

Data Availability Statement

All simulation and observed data, as well as analysis and plotting programs used in this study are available at zenodo via https://doi.org/10.5281/zenodo.7743224 (MacKay, 2023). Observed ice concentration and thickness data are also available from the Canadian Ice Service by emailing cisclients-scgclients@ec.gc.ca. Figures were produced with Matplotlib, available at https://matplotlib.org. Laplace transforms were computed online with Wolfram|Alpha (https://www.wolframalpha.com).

References

Alfrey, T. (1944). Nonhomogeneous stress in viscoelasticity. *Quarterly of Applied Mathematics, 2(2),* 113-119.

Balsamo, G., Salgado, R., Dutra, E., Boussetta, S., Stockdale, T., & Potes, M. (2012). On the contribution of lakes in predicting near –surface temperature in a global weather forecasting model. *Tellus A, 64,* 15829. https://doi.org/10.3402/tellusa.v64i0.15829

Biot, M. A. (1954). Theory of stress – strain relations in anisotropic viscoelasticity and relaxation phenomena. *Journal of Applied Physics*, *25*, 1385-1391.

Biot, M. A. (1965). *Mechanics of Incremental Deformations*. New York, NY: John Wiley and Sons Inc.

Durnford, D., Fortin, V., Smith, G., Archambault, B., Deacu, D., Dupont, F., Dyck, S., Martinez, Y., Klyszejko, E., MacKay, M., Liu, L., Pellerin, P., Pietroniro, A., Roy, F., Vu, V., Winter, B., Yu, W., Spence, C., Bruxer, J., & Dicjhout, J. (2018). Toward an operational water cycle prediction system for the Great Lakes and St. Lawrence River. *Bulletin of the American Meteorological Society*, *99*, 521-546. https://doi.org/10.1175/BAMS-D-16-0155.1

Eerola, K., Rontu, L., Kourzeneva, E., Kheyrollah Pour, H., & Duguay, C. (2014). Impact of a partly ice-free Lake Ladoga on temperature and cloudiness in an anticyclonic winter situation – a case study using a limited area model. *Tellus A*, *66*, 23929. https://doi.org/10.3402/tellusa.v66.23929

Findley, W. N., Lai, J. S., & Onaran, K. (1989). *Creep and Relaxation of Nonlinear Viscoelastic Materials*, New York, NY: Dover Publications.

Flügge, W. (ed). (1962). *Handbook of Engineering Mechanics*. New York, NY: McGraw – Hill.

Gammon P., Kiefte, H., Clouter, M., & Denner, W. (1983). Elastic constants of artificial and natural ice samples by Brillouin spectroscopy. *Journal of Glaciology, 29*, 433-460.

Gasset, N., Fortin, V., Dimitrijevic, M., Carrera, M., Bilodeau, B., Muncaster, R., Gaborit, E., Roy, G., Pentcheva, N., Bulat, M., Wang, X., Pavlovic, R., Lespinas, F., Khedhaouiria, D., & Mai, J. (2021). A 10 km North American precipitation and land-surface reanalysis based on the GEM atmospheric model. *Hydrology and Earth System Sciences*, *25*, 4917-4945. https://doi.org/10.5194/hess-25-4917-2021

Garnaud, C., MacKay, M., & Fortin, F. (2022). A one-dimensional lake model in ECCC's land surface prediction system. *Journal of Advances in Modeling Earth Systems, 14*, e2021MS002861. https://doi.org/10.1029/2021MS002861

Hetényi, M. (1946). Beams on elastic foundation. *University of Michigan Studies Scientific Series*, XVI, Ann Arbor, MI: The University of Michigan Press.

Hibler, W. D. III. (1979). A dynamic thermodynamic sea ice model. *Journal of Physical Oceanography, 9,* 815-846.

Hibler, W. D. III, & Walsh, J. (1982). On modeling seasonal and interannual fluctuations of Arctic sea ice. *Journal of Physical Oceanography, 92*, 1514-1523.

Hopkins, M. (1998). Four stages of pressure ridging. *Journal of Geophysical Research*, *103*, C10, 21883-21891.

Kirillin, G., Leppäranta, M., Terzhevik, A., Granin, N., Bernhardt, J., Engelhardt, C., Efremova, T., Golosov, S., Palshin, N., Sherstyanki, P., Zdorovennova, G., & Zdorovennov, R. (2012). Physics of seasonally ice-covered lakes: a review. *Aquatic Sciences, 74,* 659-682. https://doi.org/10.1007/s00027-012-0279-y

Le Moigne, P., Colin, J., & Decharme, B. (2016). Impact of lake surface temperatures simulated by the FLake scheme in the CNRM-CM5 climate model. *Tellus A, 68,* 31274. https://doi.org/10.3402/tellusa.v68.31274

Lee, E. H. (1955). Stress analysis in viscoelastic bodies. *Quarterly of Applied Mathematics, **13***, 183-190.

Leppäranta, M., & Wang, K. (2008). The ice cover on small and large lakes: scaling analysis and mathematical modelling. *Hydrobiologia*, *599*, 183-189. https://doi.org/10.1007/s10750-007-9201-3

MacKay, M. (2023). Ice Mechanics for 1-D Lake Models [Dataset]. Zenodo. https://doi.org/10.5281/zenodo.7743224

Mironov, D., Heise, E., Kourzeneva, E., & Terzhevik, A. (2010). Implementation of the lake parameterization scheme FLake into the numerical weather prediction model COSMO. *Boreal Environment Research*, 15, 218-230.

Parmerter, R. (1974). Dimensionless strength parameters for floating ice sheets. *AIDJEX Bulletin,* 23, 83-95.

Parmerter, R. (1975). A model of simple rafting in sea ice. *Journal of Geophysical Research,* 80, 1948-1952.

Parmerter, R., & Coon, M. (1972). Model of pressure ridge formation in sea ice. *Journal of Geophysical Research,* 77, 6565-6575.

Pietikäinen, J.-P., Markkanen, T., Sieck, K., Jacob, D., Korhonen, J., Räisänen, P., Gao, Y., Ahola, J., Korhonen, H., Laaksonen, A., & Kaurola, J. (2018). The regional climate model REMO (v2015) coupled with the 1-D freshwater lake model FLake (v1): Fenno-Scandinavian climate and lakes. *Geoscientific Model Development, 11,* 1321-1342. https://doi.org/10.5194/gmd-11-1321-2018

Rontu, L., Eerola, K., & Horttanainen, M. (2019). Validation of lake surface state in the HIRLAM v.7.4 numerical weather prediction model against in situ measurements in Finland. *Geoscientific Model Development, 12,* 3707-3723. https://doi.org/10.5194/gmd-12-3707-2019

Rothrock, D. A. (1975). The steady drift of an incompressible Arctic ice cover. *Journal of Geophysical Research, 80,* 387-397.

Schulson, E. (2004). Compressive shear faults within Arctic sea ice: fracture on scales large and small. *Journal of Geophysical Research, 109*, C07016. https://doi.org/10.1029/2003JC002108

Sjolind, S.-G. (1985). Viscoelastic buckling analysis of floating ice sheets. *Cold Regions Science and Technology, 11,* 241-246.

Staroszczyk, R. & Hedzielski, B. (2004). Creep buckling of a wedge-shaped floating ice plate. *Engineering Transactions, 52,* 111-130.

Subin, Z., Riley, W., & Mironov, D. (2012). An improved lake model for climate simulations: Model structure, evaluation, and sensitivity analyses in CESM1. *Journal of Advances in Modeling Earth Systems, 4,* M02001. https://doi.org/10.1029/2011MS000072

Verseghy, D. (2017). CLASS – The Canadian Land Surface Scheme (version 3.6.1). Technical Documentation, Environment and Climate Change Canada.